

CMOS Platform for Atomic-Scale Device Fabrication

Tomáš Škřeň¹, Nikola Pascher¹, Arnaud Garnier², Patrick Reynaud²,
Emmanuel Rolland², Aurélie Thuaire², Daniel Widmer¹,
Xavier Jehl³, Andreas Fuhrer¹

¹IBM Research – Zurich, Säumerstrasse 4, 8803 Rüschlikon, Switzerland

²Commissariat à l’Energie Atomique, Laboratoire d’Électronique des Technologies de l’Information, F38054 Grenoble, France and Université Grenoble-Alpes, F38000 Grenoble, France

³Commissariat à l’Energie Atomique, Institut Nanosciences et Cryogénie, F38054 Grenoble, France and Université Grenoble-Alpes, F38000 Grenoble, France

Abstract

Controlled atomic scale fabrication of functional devices is one of the holy grails of nanotechnology. The most promising class of techniques that enable deterministic nanodevice fabrication are based on scanning probe patterning or surface assembly. However, this typically involves a complex process flow, stringent requirements for an ultra high vacuum environment, long fabrication times and, consequently, limited throughput and device yield. Here, a device platform is developed that overcomes these limitations by integrating scanning probe based dopant device fabrication with a CMOS-compatible process flow. Silicon on insulator substrates are used featuring a reconstructed Si(001):H surface that is protected by a capping chip and has pre-implanted contacts ready for scanning tunneling microscope (STM) patterning. Processing in ultra-high vacuum is thus reduced to only a few critical steps which minimizes the complexity, time and effort required for fabrication of the nanoscale dopant devices. Subsequent reintegration of the samples into the CMOS process flow not only simplifies the post-processing but also opens the door to successful application of STM based dopant devices as a building block in more complex device architectures. Full functionality of this approach is demonstrated with magnetotransport measurements on degenerately doped STM patterned Si:P nanowires up to room temperature.

Keywords: atom-scale fabrication, dopant device, silicon-on-insulator, CMOS

1 Introduction

An early demonstration of the potential of scanning probe microscopy (SPM) in the area of atomic scale fabrication was the famous quantum coral [1]. Since then, a large number of distinct probe-based fabrication methods have been developed based either on direct atomic assembly or tip induced patterning [2]. However, broader adoption of these methods is often impeded by their inability to compete in speed and throughput with conventional lithography techniques and to find a packaging approach that allows preservation of the atomic scale devices outside an ultra high vacuum (UHV) environment.

One of the most promising SPM-based fabrication techniques is scanning tunneling microscopy (STM) based dopant device fabrication [3]. In this case, a hydrogen passivation layer on Si(001):H is locally desorbed with an STM tip in a current induced process [4, 5] to create reactive sites for selective attachment of dopant precursor molecules (see Fig. 1b and Supplementary Information). After thermal incorporation of the dopants into surface substitutional sites, overgrowth with epitaxial silicon, and ex-situ contacting of the dopant device layer, these atomically precise devices can be electrically measured in the same way as conventional semiconductor devices. The technique provides a way of defining degenerately doped metallic regions in a semiconductor with atomic-scale resolution. It allows deterministic placement of single dopant atoms [6, 7], creation of wires [8] and quantum dots [9, 10] with atomic scale dimensions and enables exploration of the quantum properties of these nanoscale systems. Furthermore, it may uniquely provide the necessary atomic precision needed for donor based quantum computing architectures [11–13].

However, as with other probe-based fabrication schemes, STM dopant device fabrication is technically extremely challenging. It requires the use of dedicated UHV equipment and the process flow for the device fabrication is very time consuming, tedious and prone to failure. As a result, only a handful of groups in the world have successfully made devices with this technique [3, 9, 14, 15], and despite efforts directed at simplifying some parts of the process [16, 17] its current application potential remains somewhat limited.

To overcome these limitations we present a platform for STM based dopant device fabrication that is fully integrated with a CMOS process flow. It drastically reduces the fabrication time and complexity, and adds additional functionalities to STM fabricated dopant devices. The key features of this platform are outlined in Fig. 1. Silicon on insulator (SOI) substrates are prepared

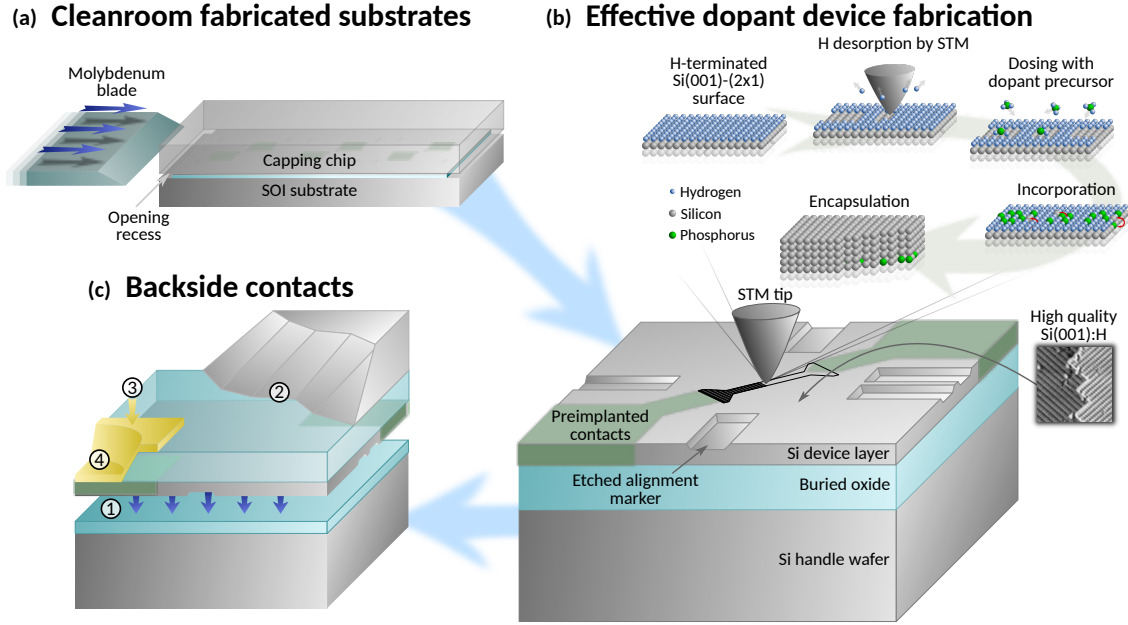


Figure 1: SOI-based platform for atomic scale dopant device fabrication. (a) Hydrogen passivated SOI substrates with pre-implanted contacts and alignment markers protected from the ambient environment by a similarly passivated capping chip that is hydrogen bonded to the sample. After loading the sample into UHV, the capping chip is removed with a molybdenum blade exposing a high quality Si(001):H surface ready for STM patterning. (b) The STM tip is aligned to the pre-implanted contacts with the help of etched alignment markers and a desired pattern is written by locally desorbing the hydrogen from the surface. Precursor gas (PH_3) selectively sticks to the dehydrogenated surface creating highly doped areas with defined geometry. After the incorporation anneal and encapsulation of the dopant device with a thin layer of Si, electrical contacts are fabricated. (c) Chip is bonded to a carrier wafer (1), original handle wafer is removed in a chemical mechanical process (2), and metal connections (3) are fabricated through vias in the buried oxide layer (4).

at wafer scale (200 mm) in a cleanroom environment using an original integration based on standard CMOS processes (see Methods). Wafers are diced into samples containing localization markers and pre-implanted contacts. Each sample is protected with a sacrificial Si capping chip, which can be easily removed inside the UHV system by inserting a molybdenum blade in the recess between the substrate and the cap. Both chips have reconstructed and hydrogen terminated Si(001):H surfaces with low defect densities directly suitable for STM patterning without the need for high-temperature in-situ surface preparation. Large implanted contact pads serve as easy-to-reach contact terminals for post-processing while shallow implant extensions come as close as 670 nm from each other and are easily accessible in the STM patterning process. After UHV fabrication and Si overgrowth, the devices can either be contacted from the top using optical or e-beam lithography or the chips can be re-integrated into the CMOS workflow using a chip-to-wafer bonding process (Fig. 1c). In the latter case, many devices can be simultaneously contacted from the backside by removal of the silicon substrate and contact can be made to the device through vias in the buried oxide (BOX) of the sample chips. Moreover, the shallow thickness (200 nm) of the SOI device layer eliminates current leakage through the substrate and allows electrical operation of STM-defined dopant devices even at room temperature.

2 Methods

SOI substrate fabrication

The pre-fabricated SOI substrates were made in a cleanroom at CEA LETI. A detailed process flow is provided in the Supplementary Information. We start with a 200 mm SOI wafer with a 200 nm thick device layer (B doped, resistivity $\sim 10 \Omega \text{ cm}$) and 400 nm thick buried oxide (BOX). In the first step we etch the alignment marks. They are 50 nm deep and sidewalls are at an angle of 55° which provides good marker visibility but does not represent a problem for scanning with the STM tip.

Contact implantation is performed in a two step process: the deep implants (fluence of $3 \times 10^{15} \text{ cm}^{-2}$ and ion energy of 20 keV and 80 keV for P and B, respectively) extend all the way through the device layer and allow contacting from the backside as required for CMOS reintegration [18]. In contrast, the shallow implants (fluence of $3 \times 10^{15} \text{ cm}^{-2}$ and ion energy of 5 keV and 12 keV for P and B, respectively) only create a 20 nm deep doped layer (before reconstruction) and limit damage to the surface due to the implantation process.

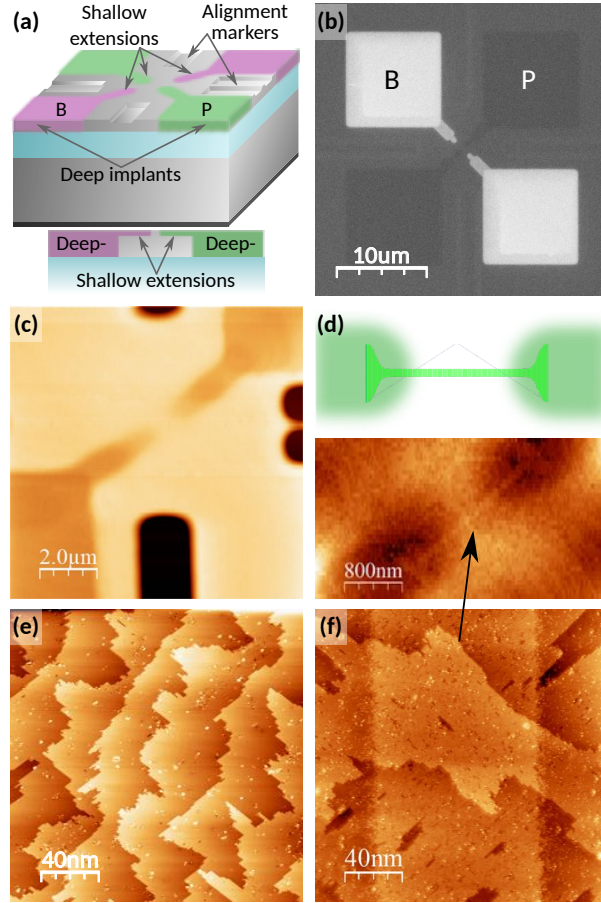


Figure 2: STM-based dopant device fabrication on an SOI sample with pre-implanted contacts. (a) Schematic of the central device region of the SOI samples with both boron (B) and phosphorus (P) implants. (b) Scanning electron microscope image of the device region with both types of implanted contacts each giving a different contrast. (c) STM image of two n-type contacts (top right to bottom left) and the three etched alignment markers (dark areas). (d) High resolution STM image of the device area showing the typical surface quality of the SOI substrates, with few residual defects that result from the de-bonding process. (e) STM image of the device area with a desorbed 30 nm wide nanowire connecting the two contacts and (f) schematic drawing of the nanowire with dimensions.

In order to achieve sufficient surface quality, retain marker geometry and limit dopant diffusion near the contact pads we use a reduced pressure chemical vapor deposition (CVD) process [19] for surface reconstruction and hydrogen termination of the SOI substrates. The surface reconstruction step is performed at a temperature of 950 °C which is sufficiently low to prevent substantial dopant diffusion. Finally, we protect the reconstructed surface by hydrophobic bonding with a sacrificial capping wafer [20]. The sandwich is then diced and the chips can be introduced into UHV for dopant device fabrication. Once capped, the samples can be kept in ambient conditions for many months without any noticeable degradation of the surface quality.

Dopant device fabrication with STM lithography

In order to handle the SOI samples in the UHV STM setup we designed a specialized sample holder that clamps the substrate from the sides allowing for easy cap removal in UHV. After introducing the sample into the system, it is first degassed for 1 h at 300 °C in order to remove adsorbed chemical species. The capping chip is removed by pressing a molybdenum blade in a recess between the sample and the cap (see Fig. S2 in the Supplementary Information). Finally, the sample is transferred to the STM stage and lithography is performed.

For this we use a commercial variable temperature STM from Omicron with custom control software and hardware. Alignment markers are used to position the tip close to the central device area which contains the contact implants (Fig. S3-5 in the Supplementary Information).

For STM imaging of the samples we typically use a sample bias of -2.5 V and tunneling current setpoint of 100 pA. In order to desorb hydrogen from the surface, we switch to writing parameters and scan over the desired areas with the feedback switched on. For patterning we apply a positive sample bias between +4.5 V and +7 V and tunneling current of around 4 nA. For slow writing of fine features we use tip velocity down to 10 nm s⁻¹, separation of lines in the desorption pattern of ~0.5 nm and voltage from the lower part of the range (+4.5 V to ~+5.5 V). For rapid, coarse patterning of large areas we use tip velocity up to 100 nm s⁻¹, line separation of ~5 nm and voltage up to +7 V. We use Python scripts to generate the desired patterns for desorption and to programmatically control the STM tip movement along the pattern.

After STM desorption of the pattern is complete, we typically image the desorbed area (or a part of it) in order to confirm desorption quality and check for desorption errors. Then we proceed with a doping procedure (similar to the one described in [9]). The sample is exposed to a 10 L dose of phosphine gas while still in the STM stage. Afterwards, the sample is transferred

to another chamber (of the same UHV system), placed on a heated manipulator and annealed to 370 °C for 1 min. After cooling the sample to a temperature of about 270 °C, a 20 nm thick layer of intrinsic Si is grown on top of the sample using a silicon sublimation source from MBE-Komponenten GmbH at growth rate of about 1 nm/min.

Sample post-processing

Compared to the conventional dopant device fabrication on bulk Si substrates, the contact fabrication procedure is facilitated by the presence of the large ($10\text{ }\mu\text{m} \times 10\text{ }\mu\text{m}$) pre-implanted contact pads. There are two possibilities for the post-processing: I) direct e-beam lithography (or, alternatively, optical lithography) contacting on a single chip level or II) reintegration of the samples in the wafer scale CMOS process flow (see Supplementary Information).

I) For the **e-beam process**, metal contacts are fabricated directly on the upper side of the samples. After overgrowth, the implanted areas are buried under a 20 nm thick layer of intrinsic Si. We first use reactive ion etching (RIE) to etch a grid of $1 \times 1\text{ }\mu\text{m}^2$ large and 50 nm deep holes into the implant pads and subsequently deposit 100 nm thick Al contacts in a standard lift-off process. The contacts are then annealed to 350 °C for 15 min in a reducing atmosphere (5% H₂, 95% Ar) at 200 mbar. In order to minimize leakage between the handle wafer (used as a gate in this case) and the device layer, we etch a frame around each device position isolating the active area from the rest of the device layer (particularly from the edges of the sample which often cause leakage). Finally, the sample is glued into a chip carrier using silver epoxy (Epotec H20e) and wire-bonded. In order to apply a gate voltage to the handle wafer, the back side of the sample is scratched with a diamond scribe prior to gluing in order to penetrate the oxide.

II) For **CMOS reintegration**, the chips are first bonded to a new handle wafer (bulk Si wafer with 200 nm oxide layer on top) with the device layer (where STM device is located) facing towards the handle wafer. The original SOI substrate is then completely removed using a chemical-mechanical process, exposing the backside of the original BOX layer. In the next step we etch vias through the BOX exposing the bottom side of the deep contact implants in the device layer. Finally, we deposit aluminum silicon alloy contacts which connect the implants through the vias to wire-bonding pads. A custom lithography step was performed on the *30 nm NW* sample to additionally define a metallic top gate. This could have been done in the reintegration step but was not foreseen in the mask-set that was used. Finally, the sample is also glued in a chip carrier and wire-bonded.

Electrical transport measurements

Transport measurements on the samples were performed using standard lock-in techniques (Signal recovery - 7265) in a four-point configuration. Low temperature measurements were carried out in a custom made variable temperature insert (VTI) cryostat allowing stable sample temperatures in a range from 2 K up to 300 K.

For the e-beam processed samples the handle wafer was used as a gate. Due to its non-degenerate doping it becomes insulating at temperatures below ~ 30 K. To circumvent this problem, we applied a short (200 ms) light pulse after every change of the gate voltage using a red LED (0402 surface mount LED, 632 nm peak wavelength) that was mounted in the chip carrier. This creates enough charge carriers to equalize the potential in the handle wafer and define a well defined voltage at the BOX interface. This was not necessary for the reintegrated samples which were equipped with a metallic gate.

3 Results and discussion

In the STM stage the pre-implanted contacts are localized using an optical microscope and large area scans that typically take less than 30 minutes (see Supplementary Information). A schematic of the device position with pre-implanted contacts is shown in Fig. 2a, whereas Fig. 2b shows a scanning electron microscopy (SEM) image of the device position. Fig. 2c shows a constant current topographic STM image taken just before defining a nanowire between two n-type contacts. The implants are clearly visible thanks to a height difference of a few monolayers (5-10) caused by different oxidation and etch rates for heavily doped Si in the surface reconstruction process after the ion implantation step. The typical quality of the Si(001):H sample surface in the central area is indicated by the STM image in Fig. 2d.

Figure 2e shows the center of the same device position with a 30 nm nanowire defined by hydrogen desorption (see Methods) with the STM tip. A dimensional representation of the nanowire pattern which was used is shown in Fig. 2f. The duration of the writing process in this case was about 15 minutes. After the writing step the sample was dosed with phosphine, annealed at 370°C for one minute to incorporate and electrically activate the dopants, overgrown with 20 nm of intrinsic Si and then removed from UHV (see Methods). This specific nanowire device was subsequently reintegrated into the 200 mm CMOS process flow for backside contact fabrication. In the following this device is referred to as *30 nm NW*.

In a similar way we fabricated a 120 nm wide nanowire with the same length of 670 nm. This second sample was post-processed using e-beam lithography and by contacting the large implant pads from the front. This sample is referred to as *120 nm NW*. A third sample containing no STM defined structures was post-processed together with the *120 nm NW* sample. Two device positions with an implant separation of 670 nm and 1170 nm were contacted and are referred to as *Blank 1* and *Blank 2*, respectively.

An important advantage of the SOI substrate is that the charge carrier density in the device layer can be tuned by application of a voltage to the silicon substrate. For samples contacted from the top by e-beam lithography we find that the presence of trapped charges at the BOX interface shifts the Fermi level in a way that leakage occurs between contacts in the device layer. By application of a negative voltage to the substrate this can be fully suppressed and the charge compensated.

In Fig. 3a we present room temperature measurements of the electrical transport through the nanowires and *Blank* positions as a function of the applied gate voltage. In the case of the *120 nm NW* and *Blank* positions the gate was realized by applying a voltage to the handle wafer, while for the reintegrated *30 nm NW* a metallic gate was lithographically defined in the post-processing step (see Supplementary Information). For the three e-beam contacted samples, the trapped charges in the BOX shift the layer into inversion. Application of a negative bias of -10 V leads to a depletion of the device layer and fully insulating behavior even at room temperature. This uniquely enables the measuring of electrical transport through STM defined dopant devices at room temperature. The situation is similar for the *30 nm NW*; however, after removal of the handle wafer in the reintegration process the Fermi level offset is not as pronounced as for the other samples and even at zero gate bias substrate leakage is small.

Figure 3b shows the resistance of the *120 nm NW* as a function of temperature. The resistance drops with decreasing temperature as expected for a metallic system and at temperatures below 25 K it increases again due to the onset of weak localization (WL) [21]. This regime is governed by enhanced backscattering from constructive interference of time-reversed paths with a length that is shorter than the phase coherence length. Resistivity is therefore sensitive to time-reversal symmetry breaking by a magnetic field and the increase in resistance is suppressed for high enough fields [22]. Figures 3d and e show in more detail the magnetoresistance of the two nanowires at different temperatures. Aside from the WL peak around $B = 0$ T, the resistance of the nanowires (particularly the *120 nm NW*) is also affected by universal conductance fluctu-

ations [21]. The relative magnitude of the WL effect in the two nanowires at 2 K is compared in Fig. 3f. The dotted lines are fits of the peaks to the 1D WL theory (see Supplementary Information). The resistivity of the *30 nm NW* and *120 nm NW* is $1.74 \text{ k}\Omega/\square$ and $1.96 \text{ k}\Omega/\square$ and the phase coherence length based on fits to WL theory is 56 nm and 54 nm, respectively. This is comparable to previously reported values [23]. The blue curve shows the situation for a reference sample with no gap between the implanted contacts where the dopants form a 3D channel with a crosssection of about $700 \times 100 \text{ nm}$. Figure 3c compares the magnitude and characteristic field of the WL effect for the three different cases. As expected, the magnitude reduces as the width and thickness of the dopant layer increases. The characteristic phase breaking field is, however, larger again for the implant case, since only the projection of the 3D scattering paths onto a plane perpendicular to the field is relevant for phase breaking. The electrical transport measurements of the dopant nanowires show consistent behavior similar to previous reports and confirm that the suggested alternative strategy for sample pre- and post-processing is compatible with the sensitive STM-based dopant device fabrication process.

4 Conclusions

In summary, we have developed a platform which integrates STM-based nanoscale dopant device fabrication in the standard CMOS process flow. Performing STM lithography on pre-implanted and hydrogen terminated SOI substrates greatly reduces the fabrication time and complexity and it facilitates sample post-processing. The thin SOI device layer suppresses substrate current leakage and, with the assistance of a gate, allows room temperature operation of the dopant devices. Last but not least, the demonstrated CMOS compatibility opens the possibility to integrate atomic scale dopant devices with additional on-chip circuitry and may in the future be extended to other STM fabricated devices such as the ones resulting from molecular assembly.

Acknowledgements

The authors gratefully acknowledge financial support from EU-FET grants SiAM 610637, PAMS 610446 and from the Swiss NCCR QSIT.

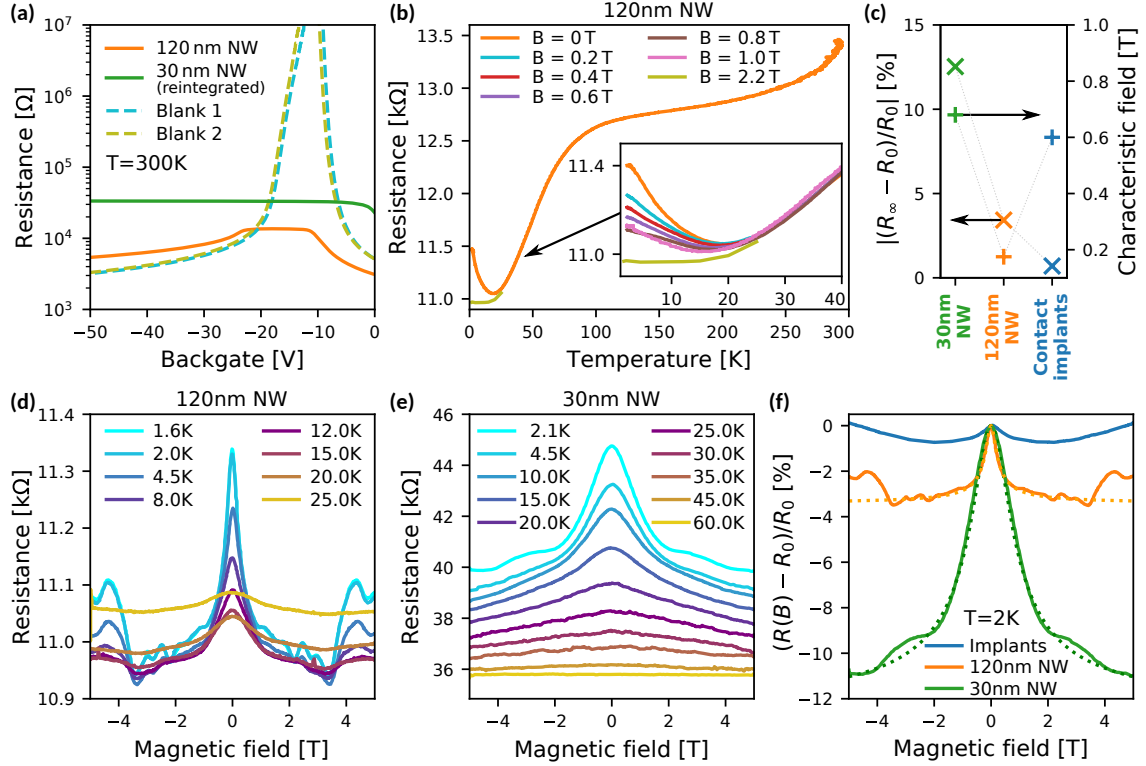


Figure 3: Electrical measurements of dopant devices fabricated on SOI substrates. (a) Room temperature resistance measurements of the 120 nm NW and 30 nm NW and two corresponding *Blank* positions as a function of gate voltage (b) Resistance of the 120 nm NW from (a) as a function of temperature from 2 K up to room temperature. Inset shows the temperature dependence measured in magnetic fields of different values. (c) Comparison of heights ($|R_\infty - R_0|/R_0$) and widths (characteristic field) of the weak localization peaks from (e). (d) Magnetoresistance of the 120 nm NW and (e) 30 nm NW measured at different temperatures. (f) Comparison of magnetoresistances of the 120 nm NW and reintegrated 30 nm NW with the magnetoresistance of implanted contacts.

References

- [1] M. F. Crommie, C. P. Lutz, and D. M. Eigler, “Confinement of Electrons to Quantum Corrals on a Metal Surface,” *Science*, vol. 262, no. 5131, pp. 218–220, oct 1993.
- [2] G. Meyer, L. Gross, and J. Repp, *Manipulation of surfaces with the methods of scanning probe microscopy*. Berlin, Heidelberg: Springer Berlin Heidelberg, 2015, pp. 67–99.
- [3] F. J. Ruess, L. Oberbeck, M. Y. Simmons, K. E. J. Goh, A. R. Hamilton, T. Hallam, S. R. Schofield, N. J. Curson, and R. G. Clark, “Toward Atomic-Scale Device Fabrication in Silicon Using Scanning Probe Microscopy,” *Nano Letters*, vol. 4, no. 10, pp. 1969–1973, oct 2004.
- [4] T. C. Shen, C. Wang, G. C. Abeln, J. R. Tucker, J. W. Lyding, P. Avouris, and R. E. Walkup, “Atomic-Scale Desorption Through Electronic and Vibrational Excitation Mechanisms,” *Science*, vol. 268, no. 5217, pp. 1590–1592, jun 1995.
- [5] R. S. Becker, G. S. Higashi, Y. J. Chabal, and a. J. Becker, “Atomic-scale conversion of clean Si(111):H-1x1 to Si(111)-2x1 by electron-stimulated desorption,” *Physical Review Letters*, vol. 65, no. 15, pp. 1917–1920, oct 1990.
- [6] M. Fuechsle, J. a. Miwa, S. Mahapatra, H. Ryu, S. Lee, O. Warschkow, L. C. L. Hollenberg, G. Klimeck, and M. Y. Simmons, “A single-atom transistor,” *Nature Nanotechnology*, vol. 7, no. 4, pp. 242–246, feb 2012.
- [7] S. R. Schofield, N. J. Curson, M. Y. Simmons, F. J. Rueß, T. Hallam, L. Oberbeck, and R. G. Clark, “Atomically Precise Placement of Single Dopants in Si,” *Physical Review Letters*, vol. 91, no. 13, p. 136104, sep 2003.
- [8] B. Weber, S. Mahapatra, H. Ryu, S. Lee, A. Fuhrer, T. C. G. Reusch, D. L. Thompson, W. C. T. Lee, G. Klimeck, L. C. L. Hollenberg, and M. Y. Simmons, “Ohm’s Law Survives to the Atomic Scale,” *Science*, vol. 335, no. 6064, pp. 64–67, jan 2012.
- [9] N. Pascher, S. Hennel, S. Mueller, and A. Fuhrer, “Tunnel barrier design in donor nanostructures defined by hydrogen-resist lithography,” *New Journal of Physics*, vol. 18, no. 8, p. 083001, jul 2016.

- [10] A. Fuhrer, M. Fuchsle, T. C. G. Reusch, B. Weber, and M. Y. Simmons, “Atomic-Scale, All Epitaxial In-Plane Gated Donor Quantum Dot in Silicon,” *Nano Letters*, vol. 9, no. 2, pp. 707–710, feb 2009.
- [11] J. L. O’Brien, S. R. Schofield, M. Y. Simmons, R. G. Clark, A. S. Dzurak, N. J. Curson, B. E. Kane, N. S. McAlpine, M. E. Hawley, and G. W. Brown, “Towards the fabrication of phosphorus qubits for a silicon quantum computer,” *Physical Review B*, vol. 64, no. 16, p. 161401, sep 2001.
- [12] L. Oberbeck, N. J. Curson, M. Y. Simmons, R. Brenner, A. R. Hamilton, S. R. Schofield, and R. G. Clark, “Encapsulation of phosphorus dopants in silicon for the fabrication of a quantum computer,” *Applied Physics Letters*, vol. 81, no. 17, pp. 3197–3199, oct 2002.
- [13] S. J. Hile, M. G. House, E. Peretz, J. Verduijn, D. Widmann, T. Kobayashi, S. Rogge, and M. Y. Simmons, “Radio frequency reflectometry and charge sensing of a precision placed donor in silicon,” *Applied Physics Letters*, vol. 107, no. 9, pp. 18–23, 2015.
- [14] E. Bussmann, M. Rudolph, G. S. Subramania, S. Misra, S. M. Carr, E. Langlois, J. Dominguez, T. Pluym, M. P. Lilly, and M. S. Carroll, “Scanning capacitance microscopy registration of buried atomic-precision donor devices,” *Nanotechnology*, vol. 26, no. 8, p. 085701, feb 2015.
- [15] G. Gramse, A. Kölker, T. Lim, T. J. Z. Stock, H. Solanki, S. R. Schofield, E. Brinciotti, G. Aeppli, F. Kienberger, and N. J. Curson, “Nondestructive imaging of atomically thin nanostructures buried in silicon,” *Science Advances*, vol. 3, no. 6, p. e1602586, jun 2017.
- [16] T.-C. Shen, J. S. Kline, T. Schenkel, S. J. Robinson, J.-Y. Ji, C. Yang, R.-R. Du, and J. R. Tucker, “Nanoscale electronics based on two-dimensional dopant patterns in silicon,” *Journal of Vacuum Science & Technology B: Microelectronics and Nanometer Structures*, vol. 22, no. 6, p. 3182, 2004.
- [17] D. R. Ward, M. T. Marshall, D. M. Campbell, T. M. Lu, J. C. Koepke, D. A. Scrymgeour, E. Bussmann, and S. Misra, “All-optical lithography process for contacting nanometer precision donor devices,” *Applied Physics Letters*, vol. 111, no. 19, p. 193101, nov 2017.
- [18] A. Thuair, P. Reynaud, C. Brun, D. Sordes, C. Carmignani, E. Rolland, X. Baillin, S. Chermamy, and G. Poupon, “Innovative Solutions for the Nanoscale Packaging of Silicon-Based

and Biological Nanowires: Development of a Generic Characterization and Integration Platform,” *IEEE Transactions on Components, Packaging and Manufacturing Technology*, vol. 6, no. 12, pp. 1804–1814, dec 2016.

- [19] J. M. Hartmann, T. Ernst, V. Loup, F. Ducroquet, G. Rolland, D. Lafond, P. Holliger, F. Laugier, M. N. Séméria, and S. Deleonibus, “Reduced pressure chemical vapor deposition of Si/Si_{1-y}Cy heterostructures for n-type metal-oxide-semiconductor transistors,” *Journal of Applied Physics*, vol. 92, no. 5, pp. 2368–2373, sep 2002.
- [20] C. Rauer, F. Rieutord, J. M. Hartmann, A.-M. Charvet, F. Fournel, D. Mariolle, C. Morales, and H. Moriceau, “Hydrophobic direct bonding of silicon reconstructed surfaces,” *Microsystem Technologies*, vol. 19, no. 5, pp. 675–679, may 2013.
- [21] C. Beenakker and H. van Houten, “Quantum Transport in Semiconductor Nanostructures,” in *Thin Solid Films*, 1991, vol. 393, no. 1-2, pp. 1–228.
- [22] B. L. Al’tshuler, A. G. Aronov, A. I. Larkin, and D. E. Khmel’nitskii, “The anomalous magnetoresistance in semiconductors,” *Sov. Phys. JETP*, vol. 54, no. 2, p. 0411, 1981.
- [23] F. J. Rueß, B. Weber, K. E. J. Goh, O. Klochan, A. R. Hamilton, and M. Y. Simmons, “One-dimensional conduction properties of highly phosphorus-doped planar nanowires patterned by scanning probe microscopy,” *Physical Review B*, vol. 76, no. 8, p. 085403, aug 2007.

Supplementary Information for: CMOS Platform for Atomic-Scale Device Fabrication

Tomáš Škřeň¹, Nikola Pascher¹, Arnaud Garnier², Patrick Reynaud²,
Emmanuel Rolland² Aurélie Thuaire², Daniel Widmer¹,
Xavier Jehl³, Andreas Fuhrer¹

¹IBM Research – Zurich, Säumerstrasse 4, 8803 Rüschlikon, Switzerland

²Commissariat à l’Energie Atomique, Laboratoire d’Électronique des Technologies de l’Information, F38054 Grenoble, France and Université Grenoble-Alpes, F38000 Grenoble, France

³Commissariat à l’Energie Atomique, Institut Nanosciences et Cryogénie, F38054 Grenoble, France and Université Grenoble-Alpes, F38000 Grenoble, France

S1 Conventional STM lithography procedure

In this section we discuss the usual procedure for dopant device fabrication on bulk Si substrates, we highlight the most time-consuming and throughput-limiting steps and compare it to the newly developed method on silicon-on-insulator (SOI) samples that was presented in the main text of the paper.

S1.1 Sample preparation

On a wafer scale, optical localization markers are defined using e-beam lithography and reactive ion etching. The wafer is then diced into 3×9 mm sized sample chips. After a standard ex-situ cleaning procedure (piranha clean for 10 min at a temperature of 80 °C, removal of the oxide using a 10 s dip in buffered hydrofluoric acid solution 7:1 and a final RCA-2 clean) the Si sample is introduced into the ultra-high vacuum (UHV) system, degassed at 500 °C for about 10 h, flashed to 1150 °C three times before hydrogen passivation in an atomic hydrogen beam (MBE Komponenten HABS II) at 325 °C. The sample is then transferred to the scanning tunneling microscope (STM) stage for dopant device fabrication. Total preparation time without the fabrication and cleaning of the sample chips takes approximately 12 hours.

In the case of the SOI substrates, very little in-situ preparation is required. After loading the sample into UHV, the capping chip is removed, a short 1 h degas at 300 °C is performed and the total time between loading the sample and STM lithography is less than 2 hours.

S1.2 STM lithography

As soon as the sample is in the STM stage, the desired areas are desorbed with the STM tip according to a predefined meander pattern. The typical STM parameters we use for scanning and STM lithography are summarized in Table S1. STM based hydrogen desorption of the active area of the nanodevice, which is typically less than a few hundred nanometers in size, only takes a few minutes or up to an hour for larger and more complex device designs. In the second step, a large contact pad has to be patterned for each electrical terminal, that can later be localized in scanning electron microscopy (SEM) and contacted with the e-beam lithography. Typical size of these pads is $1 \mu\text{m} \times 2 \mu\text{m}$ and the time required for the

Mode	Voltage [V]	Current [pA]	Speed [nm.s^{-1}]	Line width [nm]
Imaging	−(1.9-2.5)	50-500	300	-
Writing (slow, high resolution)	+4-5.2	2000-4000	10-50	0.5-2
Writing (fast, low resolution)	+5-7	2000-4000	50-100	5-10

Table S1: Typical imaging and writing STM parameters (bias measured on the sample with respect to the tip)

STM desorption is around 1-2 hours per pad. Including imaging, all required realignment steps and drift stabilization, writing of a typical dopant device therefore takes 6-8 hours.

Using the new SOI platform requires an additional initial step - precise localization of the device position and implanted contacts. This procedure is described in detail later in section S4 and the typical duration is less than 30 min. Once the implanted contacts are localized, only the active device area is desorbed and no contact pads need to be defined. This shortens the entire STM writing procedure to about an hour and allows multiple devices to be written on one chip in a single run.

S1.3 Dosing, activation anneal and overgrowth

After the STM lithographic step, the sample is dosed with the dopant precursor (typically phosphine at $p = 1.0 \times 10^{-7}$ mbar for 1 min), undergoes an activation anneal at 350 °C for one minute and then it is overgrown with a 20 nm intrinsic silicon layer. The substrate temperature during overgrowth is held at around 270 °C with the possibility to start with a so-called locking layer - to grow the first few monolayers at a lower temperature in order to prevent dopant segregation [1]. The typical growth rate is on the order of 1 nm/min. After overgrowth, the dopant device is encapsulated in the Si matrix and can be exposed to the ambient environment.

This procedure is essentially identical for the SOI samples and it takes less than an hour including temperature ramps and sample transfers between chambers.

S1.4 Sample post-processing

In order to contact the device we use e-beam lithography with several steps. In the first step, the sample is imaged with SEM to roughly localize the device. In the second step, platinum markers are defined in the vicinity of the device, and it is imaged together with the platinum markers in order to have an exact reference for its location. Then we use reactive ion etching to create an array of ~ 30 nm deep holes with a diameter of 60 nm over the contact pads to penetrate the intrinsic Si overgrowth layer. In the final step, we deposit a 90 nm thick aluminum layer to electrically contact the device terminals. The post-processing usually takes at least 3 days, possibly more, depending on logistics and tool availability. Finally, the chip is glued in a chip carrier and wire-bonded.

Post-processing is significantly different in the case of SOI substrates and is described in detail in section S2 below. The samples can be contacted either by e-beam lithography or can be reintegrated into the CMOS process flow. Both options have advantages over the conventional process. In the case of e-beam processing, no device imaging is necessary and the via etch and metal deposition steps are substantially easier due to the large size of the implants and their well defined position. This process could be conveniently performed by optical lithography as well. The CMOS reintegration process involves additional processing steps. On the other hand, it allows routine parallel processing of tens of chips at the same time and, most importantly, opens up a possibility to integrate additional circuitry and functionality to the device chips. In the device run from which data is presented in the main text, reintegration took place with many device chips but only two of them had an actual STM device on them.

S2 Full process flow for dopant device fabrication on SOI substrates

Figure S1 shows the full process flow of the dopant device fabrication on SOI substrates including substrate preparation and two alternative methods for postprocessing.

The substrate preparation is performed on a wafer scale using Deep UV lithography. The detailed structure of the markers and implants is described in section S3. After the surface reconstruction step, the wafer is capped with another wafer using hydrophobic bonding before dicing into sample chips. This requires a fine-tuning of the bonding force to a such as to withstand dicing but still make removal of the cap in UHV straightforward. With the capping chip the sample surface is protected and samples can be kept in ambient conditions basically indefinitely (sample surface quality does not show any deterioration after about a one year period). Once inserted into the vacuum, the capping chip is removed and STM lithography is performed.

The two distinct post-processing schemes are outlined in the third and fourth column of Fig. S1.

In the case of CMOS post-processing, the samples are first chemically oxidized and then bonded face-down to a new handle wafer using a hydrophilic (oxide to oxide) bonding process (the handle wafer

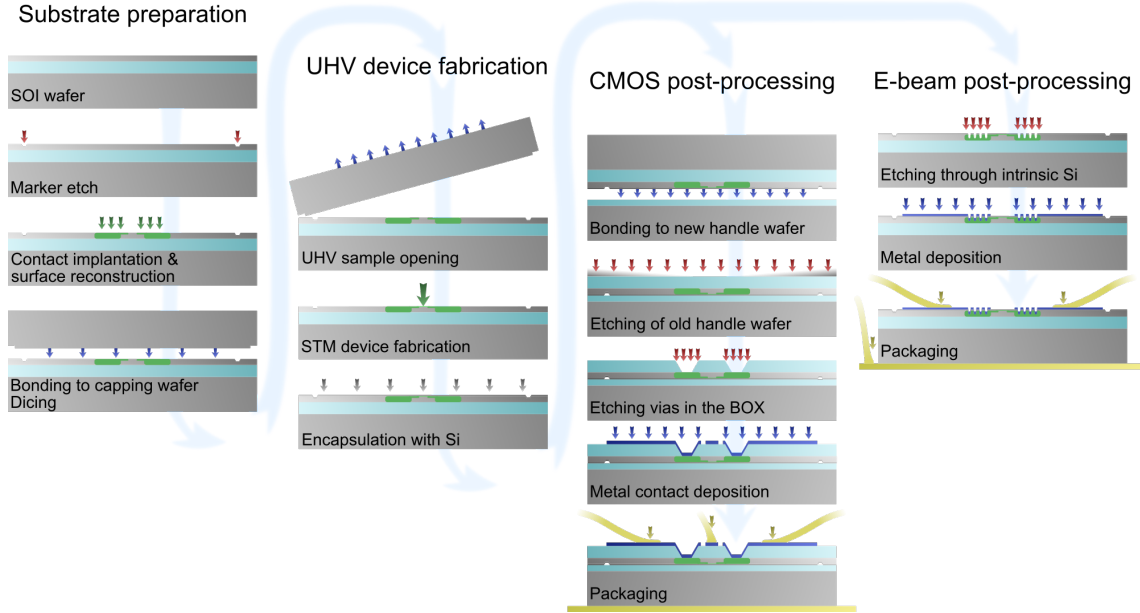


Figure S1: Outline of the process flow for dopant device fabrication on SOI substrates. After substrate preparation and capping, the sample is inserted in the UHV environment where the capping chip is removed and the STM lithographic step is performed. After encapsulation with 20 nm of Si the sample is taken out of the UHV environment and post-processed. Two distinct pathways are possible – reintegration of the samples in the CMOS process by chip-to-wafer bonding and chip level postprocessing by e-beam (or optical) lithography.

has a 200 nm layer of thermal oxide). In the next step, the original handle wafer is etched away by a chemical-mechanical polishing (CMP) process, vias penetrating the buried oxide (BOX) are etched, and metal (aluminum silicon alloy) connections to the back side of the deep contact implants are deposited. Finally, the sample is mounted in a chip carrier and bonded.

Alternatively, the sample containing the dopant devices can be processed by standard e-beam lithography, which involves etching vias through the Si overgrowth layer and depositing metal connections. Compared to the conventional process described in section S1.4, there are less lithographic steps involved and their accuracy is much less critical.

S3 Layout and characterization of the SOI substrates

Figure S2 shows the SOI substrate and the capping chip before and after opening, with optical localization markers visible. Figure S3 shows the layout of the localization markers and the implants. Each chip contains five device positions, two with a single pair of P implants, two with a single pair of B implants and one compound position with a pair of implants for both dopant types. Additionally, just below the position numbers there is a row of various testing structures, including linear implants and contact tests. Just below the number 5 there is a testing structure which is identical to P doped device positions 1 and 2 but with an implanted stripe connecting the two contacts. This testing structure was also used to evaluate the magnetoresistance of the P implants.

Figure S4a schematically depicts the structure of the pre-implanted contacts and the etched localization markers (the compound device position number 5). An actual SEM image is shown in Fig. S4b with bright B-implanted contacts and dark P-implanted contacts. The shallow implant extensions run towards the center of the device position. The distance between the opposite implants is 670 nm (position 1, 3 and P implants in position 5) or 1170 nm (position 2, 4 and B implants in position 5).

Figures S4c, d and e show typical STM micrographs of the SOI sample surface. For the STM dopant device fabrication it is critical that both the virgin silicon surface in the center of the device area as well as the implanted areas have a surface quality suitable for patterning. High implantation energies and doses were found to be detrimental for the surface, which is why we use a two-stage implantation process with high-energy deep implants for the contact pads and low-energy shallow implant extensions

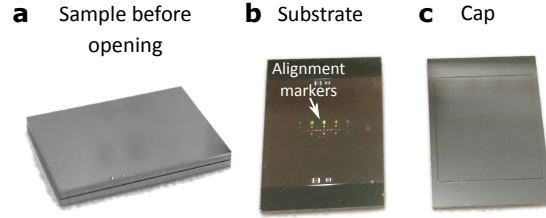


Figure S2: Photographs of the SOI substrate. **a**, Sandwich structure before opening. **b**, The substrate with alignment marks visible and **c**, the capping chip.

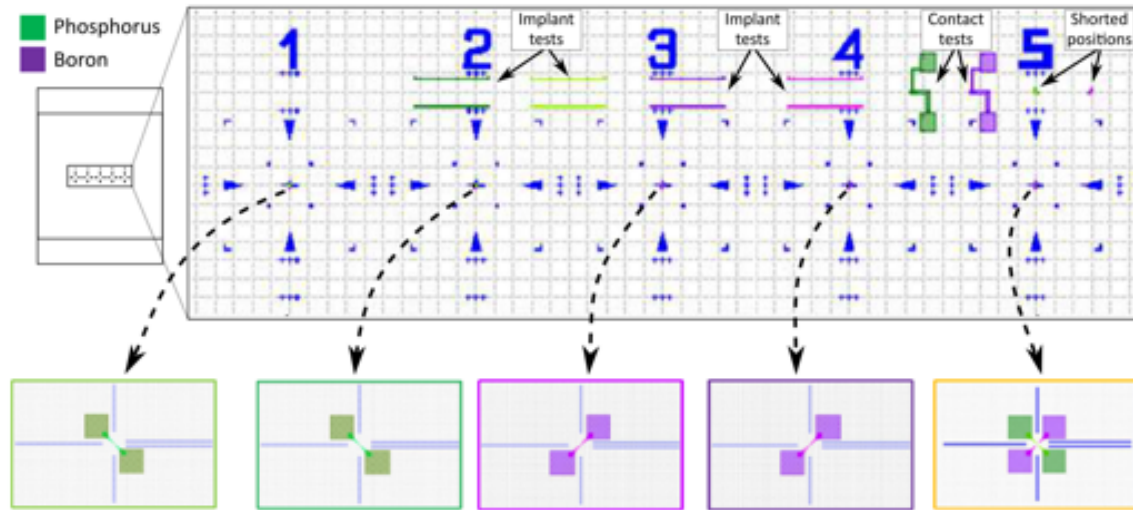


Figure S3: Detailed structure of the alignment markers and implants on an SOI substrate including 5 device positions and a number of test structures in the upper part.

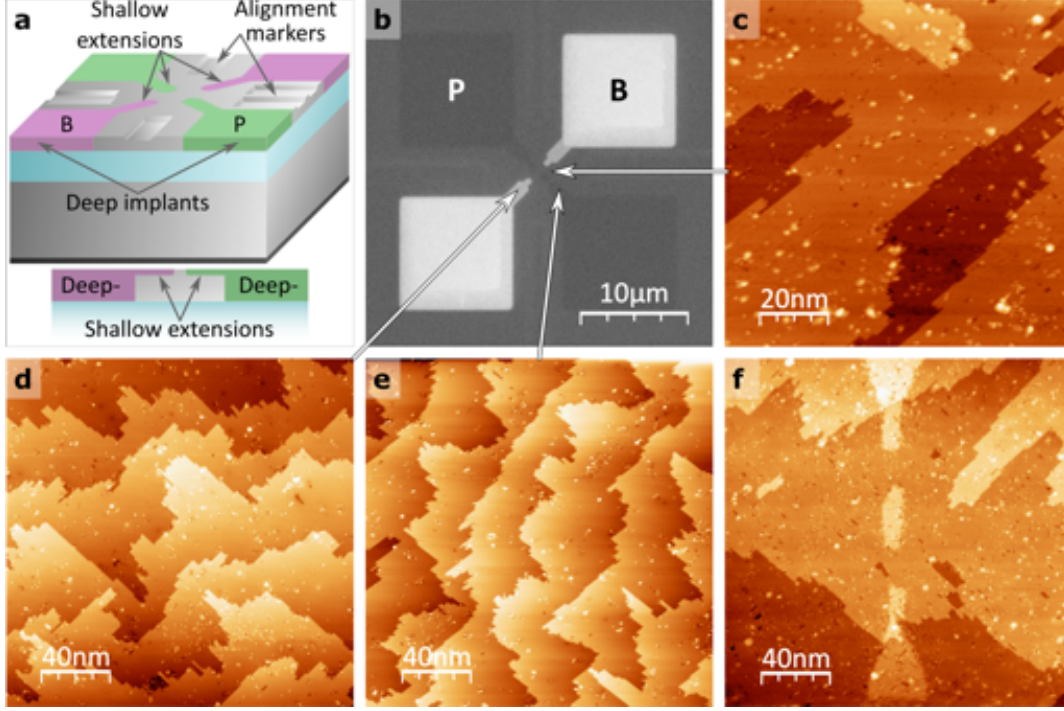


Figure S4: **a**, Structure and **b**, SEM image of the implanted contact pads acquired using the in-lens detector at 1.2 keV primary beam energy. STM images of the sample surface on the **d**, boron and **e**, phosphorus contact pad extensions that were implanted at reduced ion energy. **c**, STM image of the sample surface in the device area and **f**, an example of STM patterning on the SOI substrate.

that reach closer to the the active device area (see Fig. S4a). The deep implants (fluence of $3 \times 10^{15} \text{ cm}^{-2}$ and ion energy of 20 keV and 80 keV for P and B, respectively) extend all the way through the device layer and enable contacting from the backside as required for CMOS reintegration [2]. In contrast, the shallow implants (fluence of $3 \times 10^{15} \text{ cm}^{-2}$ and ion energy of 5 keV and 12 keV for P and B, respectively) only create a 20 nm deep doped layer and preserve the atomic scale quality of the reconstructed surface. The STM images in Fig. S4c, d and e were taken on the bare silicon and shallow P and B implants, respectively. We find the surface quality to be comparable in all three images and conclude that the shallow ion implantation does not impact surface quality on the level required for STM patterning. On the other hand, we found that surface reconstruction and hydrogen termination of the capping chip is critical for preserving atomic flatness of the sample surface. It is worth mentioning that even though we tried to tightly fix all the process parameters and waiting times, i.e., the time between surface reconstruction and bonding of the capping wafer, we still found a noticeable variability of the surface quality between different runs. This seems to indicate that extreme care during wafer handling is critical. The quality of multiple samples from a single wafer was, however, nearly identical.

The ultimate test for surface quality is, in our case, the ability to desorb the hydrogen resist with the STM. Figure S4f shows an example of a desorbed pattern (a quantum dot with two lithographically defined gaps that act as tunnel barriers) and proves that patterning of the hydrogenated SOI substrates with the STM tip and reasonable resolution is possible.

S4 Alignment and STM based dopant device fabrication on SOI substrates

A key step in dopant device fabrication is in-situ alignment to pre-fabricated structures, i.e. localization of the pre-implanted contacts with the STM. Figure S5 shows the basic steps in the localization and writing procedure.

First, the STM tip is brought close to the center of the desired device position using an optical telescope attached to the STM system (Fig. S5a). The tip is positioned to the right of the device center

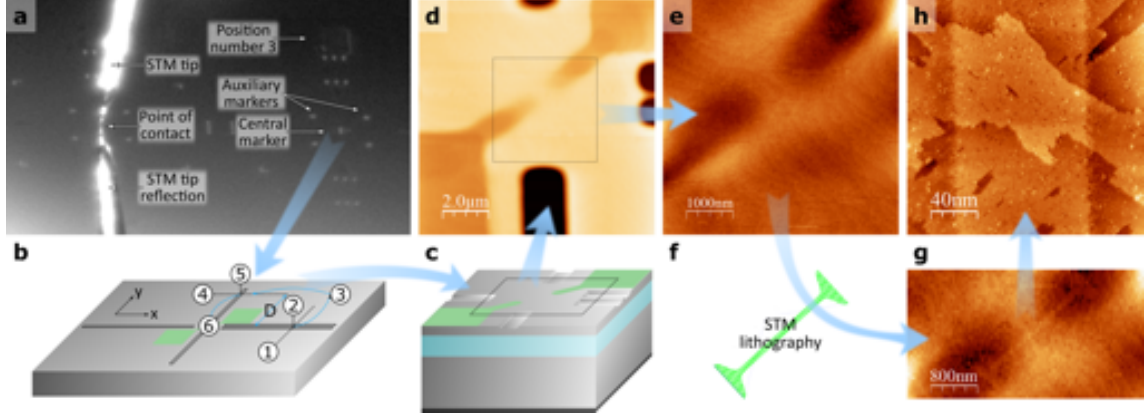


Figure S5: Optical microscope image of the SOI sample with alignment markers and STM tip visible. **a**, STM image of the typical SOI surface. **b,c**, The procedure of localization of the preimplanted contacts. STM images of device area before **d,e**, and after **g,h**, the STM lithography step.

and a full range 10 μm line scan is made in the y -direction in order to localize the alignment marker (1). Usually, the marker can be found in the first scan, otherwise we adapt the coarse y position of the tip and make another scan. After centering the y -position of the scan range to marker (2), we move the scan range by a defined number of coarse steps (D) in the y direction (3) and repeat the procedure in order to find the alignment marker in the other direction by long x -direction line scans (4). After centering the x -position of the scanner range to the alignment marker, we move the tip backwards in the y -direction ending up in the center of the device position (6). Due to hysteresis in the coarse movement of the tip and piezo creep effects there is typically an offset on the order of 1 – 2 μm between the piezo scan range center and the real device position center. With a 10 μm scanner range this is not a problem and we typically have enough freedom to access the central area for device patterning. In the future, the situation could be further improved by using a closed-loop piezo scanner.

A large overview scan is then performed (see Fig. S5d). This scan shows both the alignment markers (black areas) as well as the finger implants (brown areas). These are easily recognizable thanks to a depression that is a few monolayers deep and is a result of the cleaning procedure after the ion implantation process (because of slightly different etch rates of bare and implanted silicon). After correct positioning of the STM scanning field (Fig. S5e), desorption of the desired pattern is performed (for details see Methods). Figure S5g shows an STM image of the device position after desorbing a 120 nm wide nanowire and Fig. S5e shows a detailed image of the desorbed pattern. The total duration of the localization procedure is typically less than half an hour (from introduction of the sample into the STM stage until the start of the STM patterning) and the nanowire writing time, in this case, was only about 20 minutes. After the STM patterning step, the standard processing of the sample is performed, including dosing with phosphine, activation anneal and overgrowth with 20 nm of Si.

S5 Weak localization in dopant nanowires

The quantum correction to the Drude conductivity in the 1D regime is given by

$$\delta G_{\text{loc}}^{1\text{D}}(B) = -\frac{e^2}{2\pi\hbar} \frac{1}{L} \left(\frac{1}{D\tau_\phi} + \frac{1}{D\tau_B} \right)^{-\frac{1}{2}} \quad (1)$$

where e is electron charge, \hbar is the reduced Planck constant, L is the length of the wire, D is the diffusion constant, τ_ϕ is the phase coherence time and τ_B is the magnetic relaxation time that, for a given 1D geometry, can be calculated as

$$\tau_B = \frac{\hbar^2}{e^2} \frac{3}{W^2 D B^2}$$

where W is the wire width (in the direction perpendicular to the field and current) and B is the magnitude of the magnetic field perpendicular to the dopant device plane [3]. Using the definition of the phase

coherence length $l_\phi = \sqrt{D\tau_\phi}$ we can rewrite equation 1 as

$$\delta G_{\text{loc}}^{\text{1D}}(B) = -\alpha \frac{e^2}{2\pi\hbar} \frac{1}{L} \left(\frac{1}{l_\phi^2} + \frac{e^2 W^2 B^2}{3\hbar^2} \right)^{-\frac{1}{2}} \quad (2)$$

where α is a dimensionless correction factor that reflects the inaccuracies in the geometry. The 1D assumption in the derivation of equation 2 can be expressed by a condition that $l_\phi \gg W$. If, on the other hand, $l_\phi \ll W$ we need to apply a 2D weak localization theory which leads to a slightly different expression for the correction of the conductance [3].

Equation 2 can be used to fit the conductance of the dopant nanowires as a function of the magnetic field. Knowing the geometry of the nanowires, the only free parameters are the phase coherence length l_ϕ and the Drude conductivity σ_0 , which is the conductivity of the δ -layer without the weak localization correction, i.e. the limit of conductivity at high magnetic fields. We also fit the prefactor α but since we assume that it only reflects the inaccuracies in the wire geometry we restrict the fit to a common value for all the temperatures.

Figures S6 and S7 show the results of the fitting procedure for the two nanowires. The value of the prefactor α is in both cases close to unity, as expected (1.02 and 1.16 for the *30 nm NW* and *120 nm NW*, respectively). In general, the shape of the experimental magnetoresistance curves seems to be well captured by equation 2. The background conductivity σ_0 varies only slightly in the temperature range and the phase coherence length decreases with temperature in a similar fashion for both the nanowires, with a maximum value of about 55 nm at a temperature of 2 K (similar to previously reported value [4]).

If we compare the phase coherence length l_ϕ to the width of the nanowires W , the two values are essentially comparable for both nanowires which means that the situation can neither be considered 1D nor 2D. In this intermediate regime an analytical formula for the conductance correction is not easily obtainable. When we apply the 2D theory to the magnetoresistance curves, the quality of the fits is substantially worse but the phase coherence length we obtain is essentially the same.

In Fig. S8 we compare the phase coherence length for both nanowires. Its magnitude decreases with increasing temperature but the dependence does not follow a simple power law. At low temperatures for a 1D system, Nyquist dephasing with temperature dependence $l_\phi \sim T^{-1/3}$ is believed to be the dominant dephasing mechanism, while for higher temperatures a crossover to a 2D behavior with a steeper decrease of the l_ϕ is expected [5, 4]. This is qualitatively consistent with the trend observed in our nanowires. For low temperatures we also observe a saturation of the phase coherence length, similar to [4].

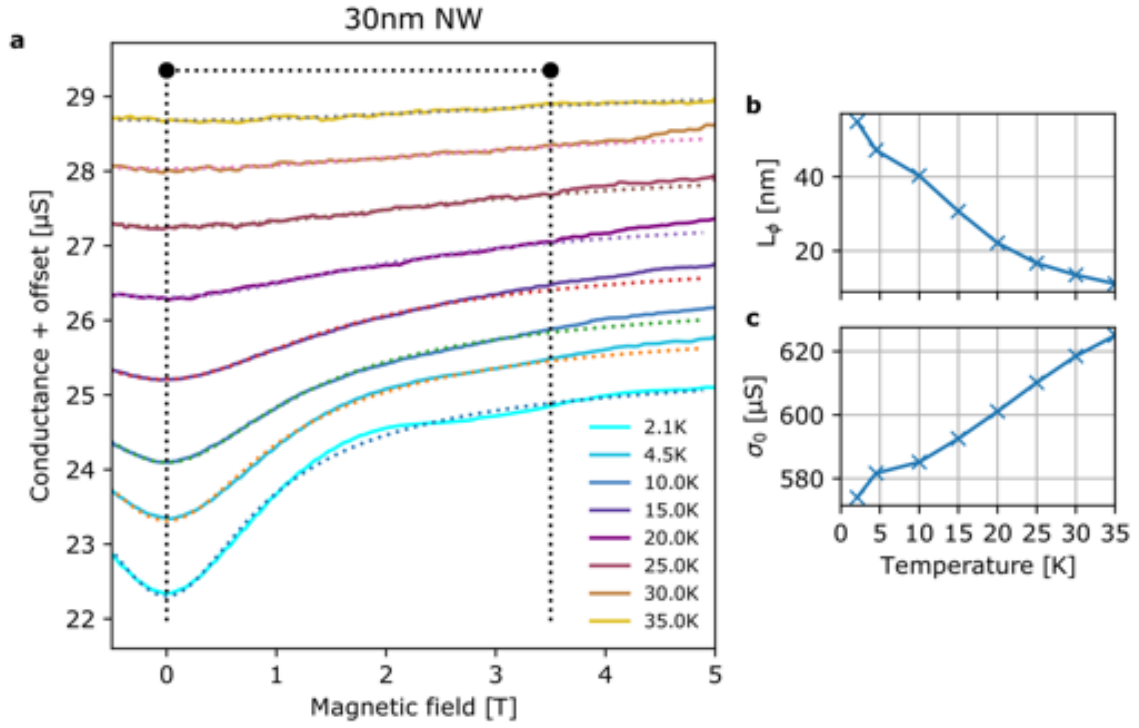


Figure S6: **a**, Magnetoresistance of the 30nm NW at different temperatures along with theoretical curves obtained by fitting the 1D weak localization formula 2. Dotted black lines show the magnetic field range used for fitting, since for large magnetic fields (above 3.5 T) pronounced universal conductance fluctuations affect the magnetoresistance. The fit parameters l_ϕ and σ_0 for each temperature are plotted in panels **b**, **c**.

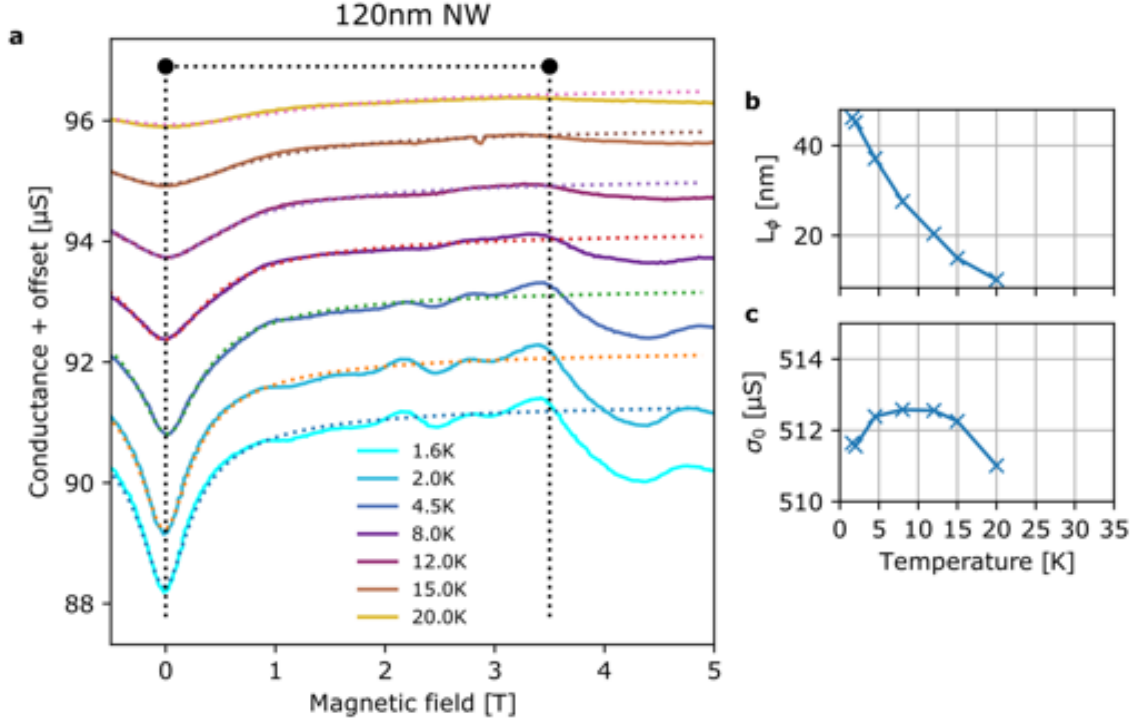


Figure S7: **a**, Magnetoresistance of the 120nm NW at different temperatures along with theoretical curves obtained by fitting the 1D weak localization formula 2. Dotted black lines show the magnetic field range used for fitting, since for large magnetic fields (above 3.5 T) pronounced universal conductance fluctuations affect the magnetoresistance. The fit parameters l_ϕ and σ_0 for each temperature are plotted in panels **b**, **c**.

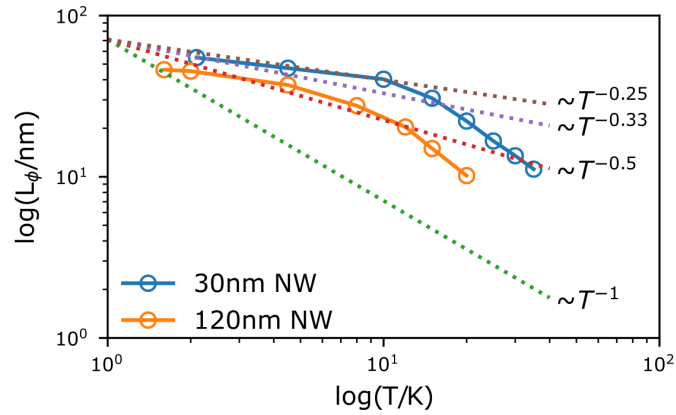


Figure S8: Log-log plot of the phase coherence length l_ϕ of the 30nm and 120nm NWs as a function of temperature obtained from the fits to formula 2. Dotted lines show the slope of power law dependencies with different exponents, for comparison.

References

- [1] J. G. Keizer, S. Koelling, P. M. Koenraad, and M. Y. Simmons, “Suppressing Segregation in Highly Phosphorus Doped Silicon Monolayers,” *ACS Nano*, vol. 9, no. 12, pp. 12 537–12 541, dec 2015.
- [2] A. Thuaire, P. Reynaud, C. Brun, D. Sordes, C. Carmignani, E. Rolland, X. Baillin, S. Cheramy, and G. Poupon, “Innovative Solutions for the Nanoscale Packaging of Silicon-Based and Biological Nanowires: Development of a Generic Characterization and Integration Platform,” *IEEE Transactions on Components, Packaging and Manufacturing Technology*, vol. 6, no. 12, pp. 1804–1814, dec 2016.
- [3] C. Beenakker and H. van Houten, “Quantum Transport in Semiconductor Nanostructures,” in *Thin Solid Films*, 1991, vol. 393, no. 1-2, pp. 1–228.
- [4] F. J. Rueß, B. Weber, K. E. J. Goh, O. Klochan, A. R. Hamilton, and M. Y. Simmons, “One-dimensional conduction properties of highly phosphorus-doped planar nanowires patterned by scanning probe microscopy,” *Physical Review B*, vol. 76, no. 8, p. 085403, aug 2007.
- [5] B. Altchuler and A. Aronov, “Electron-Electron Interaction In Disordered Conductors,” 1985, pp. 1–153.